

# Dissolution of a well-defined trichloroethylene pool in saturated porous media: Experimental design and aquifer characterization

Constantinos V. Chrysikopoulos

Department of Civil and Environmental Engineering, University of California, Irvine

Kenneth Y. Lee

Department of Civil and Environmental Engineering, Rutgers, The State University of New Jersey, Piscataway

Thomas C. Harmon

Department of Civil and Environmental Engineering, University of California, Los Angeles

**Abstract.** A unique three-dimensional bench-scale model aquifer is designed and constructed to carry out dense nonaqueous phase liquid (DNAPL) pool dissolution experiments. The model aquifer consists of a rectangular glass tank with internal dimensions 150.0 cm length, 21.6 cm width, and 40.0 cm height. The formation of a well-defined circular pool with a perfectly flat pool-water interface is obtained by a bottom plate with a precise cutout to contain the DNAPL. The aquifer is packed with a well-characterized relatively uniform sand. A conservative tracer is employed for the determination of the longitudinal and transverse aquifer dispersivities. The dissolution studies are conducted using a circular trichloroethylene (TCE) pool. The sorption characteristics of TCE onto the aquifer sand are independently determined from a flow-through column experiment. Steady state dissolved TCE concentrations at specific downstream locations within the aquifer are collected under three different interstitial velocities. An appropriate overall mass transfer coefficient is determined from each data set. The data collected in this study are useful for the validation of numerical and analytical DNAPL pool dissolution models.

## 1. Introduction

Groundwater contamination by unintentional releases of nonaqueous phase liquids (NAPLs) is a serious environmental problem. Because of their low aqueous solubilities and slow rates of dissolution into groundwater, entrapped NAPLs in the form of ganglia or pools are long-lasting sources of groundwater contamination [Geller and Hunt, 1993]. A considerable number of experimental, computational, as well as theoretical studies have focused on the dissolution of both ganglia (Powers *et al.* [1992], Imhoff *et al.* [1994], Illangasekare *et al.* [1995], Jia *et al.* [1999], and Khachikian and Harmon [2000] to mention a few) and pools [Anderson *et al.*, 1992; Johnson and Pankow, 1992; Lee and Chrysikopoulos, 1995, 1998; Holman and Javandel, 1996; Mason and Kueper, 1996; Seagren *et al.*, 1999a, b; Chrysikopoulos and Kim, 2000]. However, all of the experimental research on NAPL pool dissolution has been conducted in two-dimensional bench-scale model aquifers [Chrysikopoulos *et al.*, 1994; Pearce *et al.*, 1994; Voudrias and Yeh, 1994; Whelan *et al.*, 1994], and the behavior of NAPL pool dissolution in three-dimensional saturated porous media has not yet been investigated.

The emphasis of this work was to undertake experimental investigations to elucidate our understanding of the dissolution of single-component dense nonaqueous phase liquid

(DNAPL) pools in saturated porous media. More specifically, a three-dimensional experimental aquifer was constructed in order to investigate the transport of dissolved contaminants originating from DNAPL pools. The experimental design is unique because it allows for a constant, well-defined pool-water interface. Furthermore, the procedure for DNAPL pool formation practically eliminates the possibility of ganglia entrapment within the aquifer. The overall mass transfer coefficient for a circular trichloroethylene (TCE) pool was estimated by fitting the three-dimensional NAPL pool dissolution model derived by Chrysikopoulos [1995] to steady state dissolved TCE concentrations collected at various locations within the aquifer. All necessary transport parameters were determined independently.

## 2. Experimental Design

### 2.1. Model Aquifer Design

The bench-scale model aquifer is contained within a rectangular glass tank with internal dimensions 150 cm length, 21.6 cm width, and 40 cm height. The glass thickness is 0.95 cm. A schematic illustration of the aquifer is presented in Figure 1. The aquifer sand is separated from the upstream and downstream clear wells by specially designed screens. Each screen frame was constructed using 1.3 cm square Plexiglas bars joined together by stainless steel nuts and bolts, as shown in Figure 2. A glass tube with 0.7 cm inner diameter was inserted in the center of each clear well to approximately 5 cm above

Copyright 2000 by the American Geophysical Union.

Paper number 2000WR900082.  
0043-1397/00/2000WR900082\$09.00

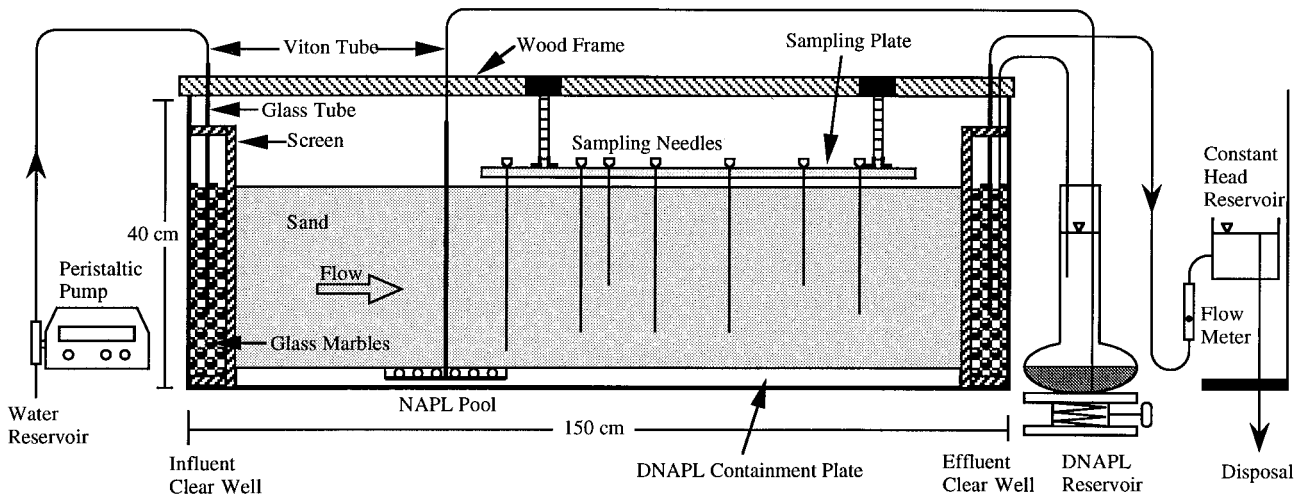


Figure 1. Schematic diagram of the bench-scale model aquifer.

the bottom of the aquifer. The flow through the model aquifer was accomplished by a Masterflex peristaltic pump (Masterflex, Chicago, Illinois). Degassed, deionized water was pumped through the glass tube into the influent clear well while maintaining a constant head at the effluent clear well. Accurate determination of the volumetric flow rate through the model aquifer was obtained by a flowmeter attached onto the outlet tube connecting the effluent clear well and the constant head reservoir.

A wood frame was placed on top of the glass tank to support the sampling plate which was constructed from a  $80 \times 17 \times 0.64$  cm Plexiglas sheet. A plan view of the sampling plate and its placement location with respect to the circular DNAPL pool is shown in Figure 3. The sampling plate contains 16 columns and 7 rows of 0.1 cm diameter holes (sampling ports) drilled on a regular  $5 \times 2.5$  cm grid. Aqueous samples from the model aquifer were collected using 20 gauge, stainless steel luer hub needles (Hamilton, Reno, Nevada). For this study, a total of seven needles were vertically inserted into the aquifer sand, and their locations are indicated in Figure 3 by the solid circles. The designation of each sampling port is specified by a lower right number, whereas the needle placement depth measured in centimeters from the bottom of the aquifer is indicated by a bold number at the upper left side of each sampling port. It should be noted that sampling ports 44 and 124 were used solely for the conservative tracer experiment. The bench-scale model aquifer was placed inside a constant temperature chamber (Forma Scientific, Marietta, Ohio) at  $20^\circ\text{C}$ .

## 2.2. DNAPL Pool Formation and Aquifer Packing

The formation of a flat DNAPL pool with a well-defined pool-water interface is a key component of the present experimental design. Previous work by Whelan *et al.* [1994] provided important information on DNAPL pool formation and dissolution within a bench-scale aquifer. However, the experimental procedures developed by Whelan *et al.* [1994] do not lead to a well-defined and flat pool-water interface. The investigators contained the DNAPL pool within a 4.7 cm deep Pyrex baking pan filled with a layer of gravel and one of sand, separated by a stainless steel mesh. The DNAPL was delivered into the bottom of the pan through a vertically inserted glass pipet. Formation of residual DNAPL ganglia in the upper half of the

Pyrex pan may occur as the injected DNAPL displaces the interstitial water from the gravel layer and the overburden sand contained within the pan. Accurate determination of the pool-water interfacial area resulting from this setup is not a trivial task. Furthermore, intrusion of a glass pipet in the aquifer may disturb the interstitial flow. These flaws are resolved by a newly designed bottom plate, which permits the formation of a specified pool-water interface and uniform horizontal flow within the model aquifer.

The bottom plate is a  $127 \times 19 \times 0.64$  cm aluminum sheet. A 0.5 cm deep, circular disk with 7.6 cm diameter was removed from the aluminum sheet in order to form the experimental pool, as shown in Figure 4a. The aluminum sheet was anodized to avoid corrosion, and the bottom of the pool was covered with a 0.08 cm thick Teflon sheet. Holes of 0.2 cm diameter were drilled into the Teflon sheet 1.0 cm apart in the form of a square matrix. A 0.5 cm diameter glass bead was placed on top of each hole. This matrix of beads supported a circular #60 stainless steel mesh, which prevented settling of sand into the pool. The void volume of the particular pool was estimated to

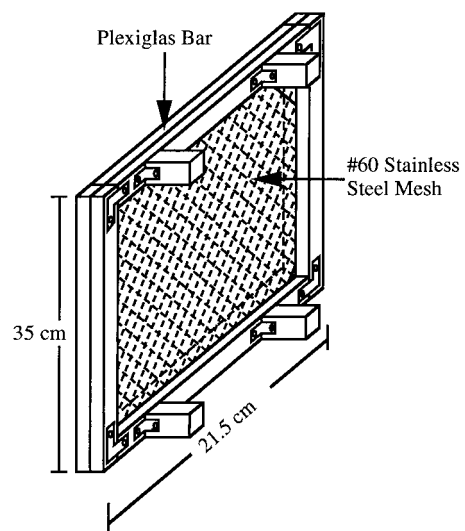
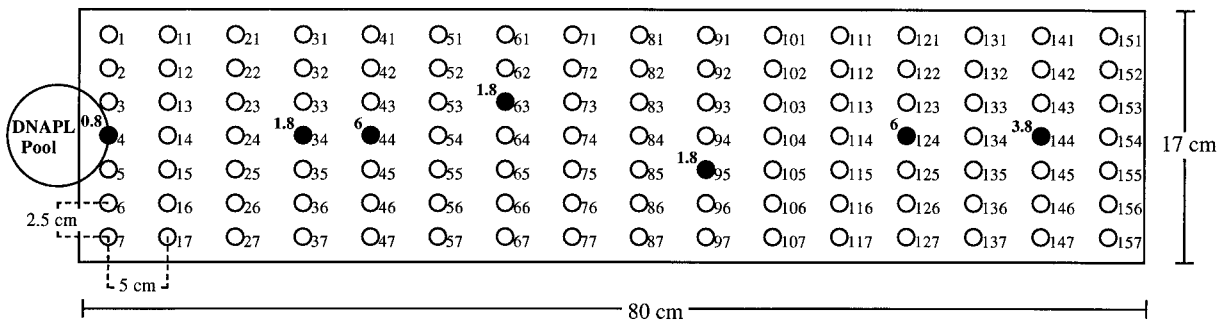


Figure 2. Schematic illustration of a clear well screen.



**Figure 3.** Schematic diagram of the sampling plate and sampling ports. Solid circles represent the needle placement locations. For each solid circle, the lower right number indicates the sampling port number, and the upper left bold number indicates the needle placement depth measured in centimeters from the bottom of the aquifer.

be approximately 12 mL. A *y-z* cross section of the bottom plate along the center of the pool is shown in Figure 4b. The bottom plate was placed inside the glass tank, and its edges were sealed with plumber’s putty to avoid preferential flow beneath or along the sides of the plate.

The DNAPL, trichloroethylene (TCE), was delivered into the pool through a 16 gauge stainless steel tube. The tube was inserted into the pool through a horizontal hole drilled along the aluminum sheet, as illustrated in Figure 4. The stainless steel tube was connected to a DNAPL reservoir through a Viton tube with 0.16 cm inner diameter (Masterflex, Chicago, Illinois). A 500 mL volumetric flask containing approximately 80 mL of TCE and 400 mL of water served as the DNAPL reservoir. The flask was placed on a vertically adjustable jack. The water head inside the DNAPL reservoir and inside the model aquifer was balanced by connecting a separate Viton

tube from the effluent clear well to the water inside the DNAPL reservoir (see Figure 1). The amount of DNAPL inside the pool was controlled by adjusting the height of the DNAPL reservoir. It should be noted that the experimental design of the well-defined DNAPL pool formation was proven successful. Preliminary experiments with the rectangular glass tank filled with water in the absence of sand verified that all water is displaced from the experimental pool cavity by TCE and a well-defined TCE-water interface is formed.

The model aquifer was packed, in 1–2 cm lifts, with kiln-dried Monterey sand (RMC Lonestar, Monterey, California) to a total depth of ~15 cm. The sand was packed under a 5 cm water head. Only the sand fraction which passed the #40 sieve (0.425 mm) but was retained on the #60 sieve (0.250 mm) was used. The parameters of the particular sand fraction used in the model aquifer were evaluated separately by gravimetric

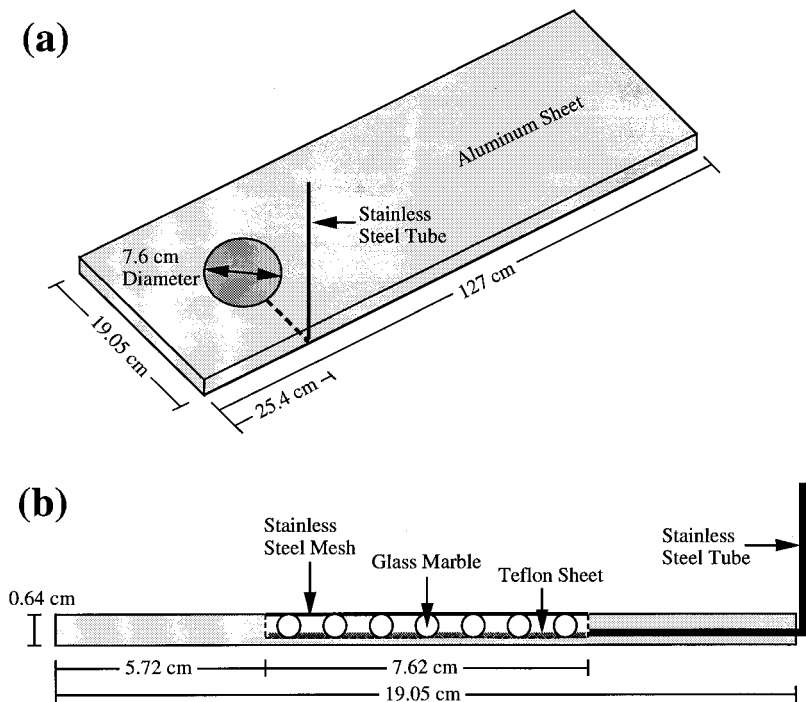


**Figure 4.** (a) Isometric view of the aluminum bottom plate showing the pool location. (b) The *y-z* cross section of the bottom plate through the center of the pool showing the detailed pool design and the shape of the stainless steel tube.

procedures. The dry bulk density of the sand was determined to be  $\rho_b = 1.61$  kg/L, and the porosity was determined to be  $\theta = 0.415$ . Furthermore, a mechanical vibrating device was employed in order to obtain a uniform packing within the model aquifer. Glass marbles with 1.9 cm diameter were added into the influent and effluent clear wells to balance the sand pressure exerted on the screens. Following the installation of the sampling plate, seven sampling needles were carefully inserted into the model aquifer. The needles were affixed to the sampling plate with silicon adhesive. The water elevation within the model aquifer was adjusted to a desired level by controlling the water elevation in the influent and effluent clear wells. An aqueous solution containing approximately 200 mg/L of the biological inhibitor sodium azide was delivered into the influent clear well by a peristaltic pump. The addition of sodium azide prevented any possible biological degradation of TCE and fouling of the system.

### 3. Tracer Experiment

Prior to the DNAPL delivery into the pool a tracer experiment was conducted under steady flow conditions in order to determine the longitudinal and transverse dispersivities of the three-dimensional model aquifer. Bromide ion ( $\text{Br}^-$ ), in the form of the moderately soluble potassium bromide salt (KBr), was the conservative inorganic tracer employed in this study. Alkali halides are the most commonly used salts for subsurface fluid tracing [Chrysikopoulos, 1993]. Note that the injected tracer source concentration should be low enough to avoid any density effects and gravity segregation, yet high enough to ensure tracer detection by the analytical technique of choice. Ion chromatography was employed in this study (Dionex Series 4000i, Sunnyvale, California).

A source solution containing 2.04 g/L of KBr (1.37 g/L of Br) was injected into the model aquifer via a syringe pump through the needle located at sampling port 44 (see Figure 3). The tip of the needle represents a point source geometry. The tracer was injected with a constant and relatively slow rate (1.2 mL/h) so that the flow field within the model aquifer was not disturbed. Sampling port 124 was used to periodically collect 0.3 mL samples of the interstitial liquid. Because the fluid within the sampling needles does not equilibrate fast enough with the local solution within the model aquifer, 0.1 mL of interstitial fluid was purged and discarded from the sampling needle just before each sample collection.

The transport of a conservative solute in saturated, homogeneous porous media, accounting for three-dimensional hydrodynamic dispersion in a uniform flow field, is governed by the following partial differential equation:

$$\begin{aligned} \frac{\partial C(t, x, y, z)}{\partial t} - D_x \frac{\partial^2 C(t, x, y, z)}{\partial x^2} - D_y \frac{\partial^2 C(t, x, y, z)}{\partial y^2} \\ - D_z \frac{\partial^2 C(t, x, y, z)}{\partial z^2} + U_x \frac{\partial C(t, x, y, z)}{\partial x} \\ = F(t, x, y, z), \end{aligned} \quad (1)$$

where  $C$  is the liquid phase solute concentration;  $D_x$ ,  $D_y$ , and  $D_z$  are the longitudinal, lateral, and vertical hydrodynamic dispersion coefficients, respectively;  $U_x$  is the average interstitial velocity;  $F$  is a general functional form of the source configuration;  $t$  is time; and  $x$ ,  $y$ , and  $z$  are the spatial coordinates in the longitudinal, lateral, and vertical directions, respectively.

The dispersion coefficients are defined as [Bear and Verruijt, 1987, p. 164]

$$D_x = \alpha_L U_x + \mathcal{D}_e, \quad (2)$$

$$D_y = D_z = \alpha_T U_x + \mathcal{D}_e, \quad (3)$$

where  $\alpha_L$  and  $\alpha_T$  are the dispersivities in the longitudinal and transverse directions, respectively, and  $\mathcal{D}_e = \mathcal{D}/\tau^*$  is the effective molecular diffusion coefficient (where  $\mathcal{D}$  is the molecular diffusion coefficient and  $\tau^* > 1$  is the tortuosity coefficient). A time-dependent point source configuration in a three-dimensional aquifer is represented by

$$F(t, x, y, z) = \frac{G(t)}{\theta} \delta(x - x_0) \delta(y - y_0) \delta(z - z_0), \quad (4)$$

where  $G$  represents the tracer mass release rate;  $\theta$  is the porosity;  $\delta$  is the Dirac delta function; and  $x_0$ ,  $y_0$ ,  $z_0$  represent the  $x$ ,  $y$ ,  $z$  Cartesian coordinates of the point source, respectively.

The appropriate initial and boundary conditions for the case of an aquifer with infinite longitudinal and lateral directions and finite vertical thickness are as follows

$$C(0, x, y, z) = 0, \quad (5)$$

$$C(t, \pm\infty, y, z) = 0, \quad (6)$$

$$C(t, x, \pm\infty, z) = 0, \quad (7)$$

$$\frac{\partial C(t, x, y, 0)}{\partial z} = 0, \quad (8)$$

$$\frac{\partial C(t, x, y, H)}{\partial z} = 0, \quad (9)$$

where  $H$  is the average water-saturated aquifer thickness (in this study,  $H$  represents the average of the thicknesses observed at the influent and effluent clear wells), the vertical level  $z = 0$  defines the location of the water table, and  $z$  increases in the downward direction. The condition (5) corresponds to the situation in which solutes are initially absent from the three-dimensional porous formation, (6) and (7) indicate that the aquifer is infinite horizontally and laterally, boundary condition (8) represents a zero dispersive flux boundary, and (9) implies that the aquifer is confined by an impermeable layer at depth  $z = H$ .

The governing transport equation (1) subject to conditions (5)–(9) is solved analytically by employing Laplace, Fourier, and finite Fourier cosine transform techniques following the procedures presented by Sim and Chrysikopoulos [1999]. The desired solution is given by

$$\begin{aligned} C(t, x, y, z) = & \left( \frac{1}{16\pi^2 D_x D_y} \right)^{1/2} \int_0^t \frac{G(t-\tau)}{\theta\tau} \\ & \cdot \exp \left[ \frac{U_x(x-x_0)}{2D_x} - \frac{1}{4\tau} \left( \frac{(x-x_0)^2}{D_x} + \frac{(y-y_0)^2}{D_y} \right) - \frac{U_x^2\tau}{4D_x} \right] \\ & \cdot \left\{ \frac{1}{H} + \frac{2}{H} \sum_{m=1}^{\infty} \exp \left[ - \left( \frac{m\pi}{H} \right)^2 D_z \tau \right] \right. \\ & \cdot \left. \cos \left( \frac{m\pi z}{H} \right) \cos \left( \frac{m\pi z_0}{H} \right) \right\} d\tau, \end{aligned} \quad (10)$$

where  $m$  is an integer summation index.

The average water velocity within the model aquifer can be determined by

$$U_x = \frac{Q}{wH\theta}, \quad (11)$$

where  $Q$  is the water volumetric flow rate generated by the peristaltic pump and  $w$  is the aquifer width. For  $Q = 552$  mL/h,  $w = 21.6$  cm,  $H = 12.6$  cm, and  $\theta = 0.415$ , the interstitial velocity in the model aquifer during the tracer experiment was evaluated to be  $U_x = 4.9$  cm/h. The tracer experiment was conducted under a relatively high interstitial velocity in order to ensure that the hydrodynamic dispersion is governed mainly by mechanical dispersion and the contribution of the effective diffusion coefficient for bromide,  $\mathcal{D}_e^{\text{Br}}$ , is minimum. Furthermore, under the present experimental conditions the walls of the rectangular glass tank are not encountered by the tracer.

For the experimental parameters of the tracer test ( $G = 1.64$  mg/h,  $U_x = 4.9$  cm/h,  $H = 12.6$  cm,  $\theta = 0.415$ ,  $x_0 = 20.0$  cm,  $y_0 = 0.0$  cm, and  $z_0 = H - 6.0 = 6.6$  cm) the nonlinear least squares regression program PEST [Doherty et al., 1994] was employed to estimate the hydrodynamic dispersion coefficients  $D_x = 1.31$  cm<sup>2</sup>/h and  $D_y = D_z = 0.144$  cm<sup>2</sup>/h by fitting the analytical solution (10) to the breakthrough bromide concentrations observed at sampling port 124. Figure 5 clearly shows a good agreement between the experimental data (circles) and the simulated concentration history (solid curve). In view of  $\mathcal{D}_e^{\text{Br}} = 7.24 \times 10^{-2}$  cm<sup>2</sup>/h [Domenico and Schwartz, 1990] and assuming  $\tau^* = 1.43$  for sand [de Marsily, 1986], the desired model aquifer dispersivities  $\alpha_L = 0.259$  cm and  $\alpha_T = 0.019$  cm are evaluated from (2) and (3), respectively. For the scale of the present experiment this value for  $\alpha_L$  is very reasonable when compared to the scale-dependent longitudinal dispersivity data compiled by Gelhar [1986].

#### 4. Column Experiment

A column flow-through experiment was conducted in order to characterize the interaction of aqueous phase TCE with the model aquifer sand. A 25.0 cm long borosilicate glass column (Omnifit, Cambridge, England) with 2.5 cm inner diameter was packed with the same sand used in the model aquifer under a constant upflow of deionized water. Two syringe infusion

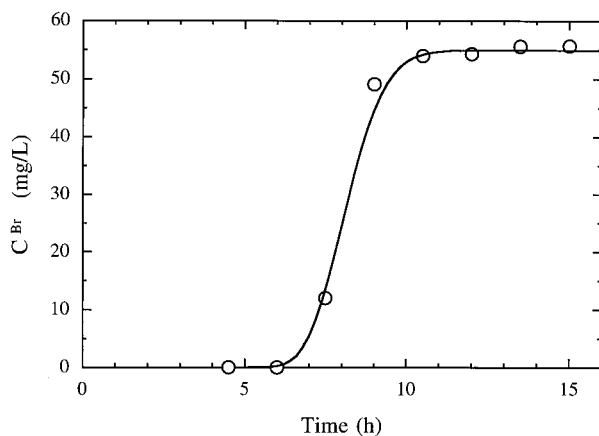


**Figure 5.** Bromide concentration breakthrough data observed at sampling location 124 (circles) and simulated concentration history (solid curve).

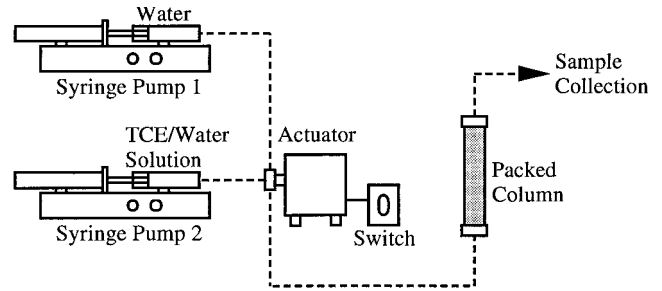


**Figure 6.** Schematic diagram of the experimental column apparatus.

pumps (model KDS200) were used, one for delivering deionized water to the column, and the other for delivering the TCE-water solution. The injected aqueous phase TCE concentration was 156.6 mg/L, and the volumetric flow rate through the column was 20.4 mL/h, which corresponds to an interstitial velocity of 10.02 cm/h. A switching valve (Upchurch Scientific, Oak Harbour, Washington) was used to alter the flow between the two pumps. A schematic diagram of the column experimental setup is shown in Figure 6.

Effluent samples of approximately 0.5 mL volume were collected periodically into receiving vials containing 1 mL of pentane. The TCE concentrations of the effluent samples were determined by standard gas chromatography (Hewlett-Packard model 5890 with electron capture detector, Fullerton, California). It was assumed that the sorption of aqueous phase TCE onto the sand is a linear, reversible, and instantaneous process. The nonlinear least squares regression program PEST [Doherty et al., 1994] was employed to estimate the longitudinal hydrodynamic dispersion coefficient,  $D = 0.785$  cm<sup>2</sup>/h, and the retardation factor,  $R = 1.31$ , by fitting an available analytical solution describing one-dimensional solute transport in homogeneous, saturated porous media [Lindstrom et al., 1967; Gershon and Nir, 1969] to the TCE breakthrough experimental data. For the porosity and density of the model aquifer ( $\theta = 0.415$  and  $\rho_b = 1.61$  kg/L) this value of  $R$  corresponds to sand-water distribution coefficient ( $K_d$ ) of 0.08 mL/g. The simulated concentration breakthrough curve as well as the experimental data are shown in Figure 7.

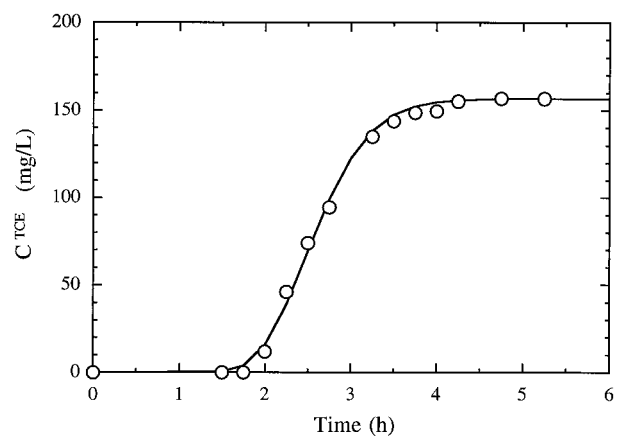


**Figure 7.** Aqueous phase TCE concentration breakthrough data collected at the end of the column (circles) and simulated concentration history (solid curve) for  $Q = 20.4$  mL/h.

**Table 1.** Observed Dissolved TCE Concentrations and Estimated  $k^*$  Values

Location, † cm			Experiment 1 $U_x = 0.75$ cm/h		Experiment 2 $U_x = 1.96$ cm/h		Experiment 3 $U_x = 0.25$ cm/h		
Port	$x$	$y$	$z$	$t = 237$ hours	$t = 264$ hours	$t = 120$ hours	$t = 144$ hours	$t = 720$ hours	$t = 888$ hours
4	0.0	0.0	0.8	417.5	390.0	233.4	240.5	627.0	629.2
34	15.0	0.0	1.8	117.6	91.3	77.4	86.7	206.1	202.4
63	30.0	2.5	1.8	82.2	78.7	54.5	54.9	154.9	148.5
95	45.0	-2.5	1.8	143.5	145.8	51.3	51.2	141.4	141.1
144	70.0	0.0	3.8	43.0	44.2	17.4	17.9	71.8	70.3
$k^*$ , cm/h				$0.0381 \pm 0.004$	$0.0378 \pm 0.004$	$0.0473 \pm 0.003$	$0.0474 \pm 0.003$	$0.0268 \pm 0.002$	$0.0267 \pm 0.002$

Observed dissolved TCE concentrations are given in mg/L. The time given is since the initiation of each individual experiment.

†The origin of the coordinate system is at the bottom of port 4.

## 5. TCE Pool Dissolution Experiments

The interstitial velocity was initially maintained at 0.75 cm/h. The first experiment began when 12 mL of TCE was pumped from the DNAPL reservoir into the pool at a rate of 180 mL/h. The elevation of the TCE reservoir was carefully adjusted so that the TCE-water interface in the reservoir was at the same level as the pool-water interface in the model aquifer. During the TCE transfer into the pool a fraction of the injected TCE dissolved into the water that initially occupied the pool. This volume of water was displaced into the aquifer by the intruding TCE, causing an undesired spike of aqueous phase TCE concentration in the model aquifer. Because of this inherent experimental artifact, early time dissolution data were considered biased and are not presented here. Consequently, aqueous samples were collected only after the dissolved TCE concentrations within the model aquifer had achieved a quasi-steady state.

Interstitial liquid samples were collected from sampling ports 4, 34, 63, 95, and 144 at approximately 237 hours after the first TCE pool dissolution experiment began. The samples were collected with disposable, 1 mL tuberculin syringes (Becton Dickinson & Co., New Jersey). Approximately 0.1 mL of the interstitial fluid was purged and discarded from each sampling needle just before the collection of 0.3 mL liquid sample. Preliminary testing indicated that 0.3 mL afforded a practical detection limit while minimizing hydrodynamic disturbances and perturbations from steady state dissolution conditions. Although sample collection from additional ports is desirable, it may lead to unreliable dissolved concentration data. Each sample was immediately transferred into a receiving vial. The details of the sample analysis are presented later in this section. A second set of interstitial liquid samples were collected 27 hours after the first sampling time. Subsequently, the interstitial velocity was increased to 1.96 cm/h, and two additional sets of interstitial liquid samples were collected at 120 and 144 hours after the initiation of the second experiment. Finally, the interstitial velocity was adjusted to 0.25 cm/h, and two sets of interstitial liquid samples were collected at 720 and 888 hours after the initiation of the third experiment. All of the aqueous phase TCE concentrations observed at the specified sampling locations are listed in Table 1. Considering experimental error associated with the sampling and extraction behavior, the two data sets collected for each interstitial velocity considered in this study appear to be quite similar, confirming that the pool dissolution had achieved steady state conditions.

The transient contaminant transport from a dissolving DNAPL circular pool in a three-dimensional, homogeneous

porous medium under steady state uniform flow, assuming that the dissolved organic sorption is linear and instantaneous, is governed by

$$R \frac{\partial C(t, x, y, z)}{\partial t} = D_x \frac{\partial^2 C(t, x, y, z)}{\partial x^2} + D_y \frac{\partial^2 C(t, x, y, z)}{\partial y^2} + D_z \frac{\partial^2 C(t, x, y, z)}{\partial z^2} - U_x \frac{\partial C(t, x, y, z)}{\partial x} - \lambda RC(t, x, y, z), \quad (12)$$

where  $R$  is the retardation factor and  $\lambda$  is a first-order decay constant. Assuming that NAPL pool dissolution is described by the following mass transfer relationship, applicable at the NAPL-water interface [Chrysikopoulos, 1995],

$$-\mathcal{D}_e \frac{\partial C(t, x, y, 0)}{\partial z} = k(t, x, y)[C_s - C(t, x, y, \infty)], \quad (13)$$

where  $k(t, x, y)$  is the local mass transfer coefficient dependent on time and location on the NAPL-water interface,  $C_s$  is the aqueous saturation (solubility) concentration, and  $C(t, x, y, \infty) \approx 0$  corresponds to the contaminant concentration outside the boundary layer, the appropriate initial and boundary conditions for this system are

$$C(0, x, y, z) = 0, \quad (14)$$

$$C(t, \pm\infty, y, z) = 0, \quad (15)$$

$$C(t, x, \pm\infty, z) = 0, \quad (16)$$

$$\mathcal{D}_e \frac{\partial C(t, x, y, 0)}{\partial z} = \begin{cases} -k(t, x, y)C_s & (x - \ell_{x_0})^2 + (y - \ell_{y_0})^2 \leq r^2, \\ 0 & \text{otherwise,} \end{cases} \quad (17)$$

$$C(t, x, y, \infty) = 0, \quad (18)$$

where  $\ell_{x_0}$ ,  $\ell_{y_0}$  indicate the  $x$ ,  $y$  Cartesian coordinates of the pool origin, respectively, and  $r$  is the pool radius. The concentration boundary layer implies that the dissolved concentration changes from the solubility concentration at the DNAPL-water interface to the free-stream concentration in the interstitial fluid [Bennett and Myers, 1982; Chrysikopoulos and Lee, 1998]. It should be noted that the decay term  $\lambda RC$  in the governing equation (12) indicates that the total concentration (aqueous plus sorbed solute mass) disappears due to possible decay or biological/chemical degradation. In this study it was assumed

that the mass transfer coefficient is equal to the corresponding time-invariant overall mass transfer coefficient ( $k^* = k(t, x, y)$ ). This is a reasonable assumption for steady state physico-chemical and hydrodynamic conditions [Chrysikopoulos and Lee, 1998].

The analytical solution to the governing partial differential equation (12) subject to conditions (14)–(18) has been derived by Chrysikopoulos [1995] as follows:

$$C(t, x, y, z) = \frac{C_s k^*}{2\pi \mathcal{D}_e} \int_0^t \int_{\mu_1}^{\mu_2} \left(\frac{D_z}{R\tau}\right)^{1/2} \exp\left[-\lambda\tau - \frac{Rz^2}{4D_z\tau}\right] \cdot \exp[-\mu^2\{\text{erf}[n_2] - \text{erf}[n_1]\}] d\mu d\tau, \quad (19)$$

where

$$\mu_1 = (y - \ell_{y_0} + r) \left(\frac{R}{4D_y\tau}\right)^{1/2}, \quad (20)$$

$$\mu_2 = (y - \ell_{y_0} - r) \left(\frac{R}{4D_y\tau}\right)^{1/2}, \quad (21)$$

$$n_1 = \left\{x - \frac{U_x\tau}{R} - \ell_{x_0} + [r^2 - (v - \ell_{y_0})^2]^{1/2}\right\} \left(\frac{R}{4D_x\tau}\right)^{1/2}, \quad (22)$$

$$n_2 = \left\{x - \frac{U_x\tau}{R} - \ell_{x_0} - [r^2 - (v - \ell_{y_0})^2]^{1/2}\right\} \left(\frac{R}{4D_x\tau}\right)^{1/2}, \quad (23)$$

$$v = y - \mu \left(\frac{4D_y\tau}{R}\right)^{1/2}, \quad (24)$$

where  $\mu$  and  $\tau$  are dummy integration variables. Although the analytical solution was derived assuming infinite lateral dimensions, it is applicable for this study because under the present experimental conditions the walls of the rectangular glass tank are not encountered by the dissolving plume.

The TCE solubility limit is  $C_s = 1100$  mg/L [Mackay et al., 1992], and the molecular diffusion coefficient  $\mathcal{D}^{\text{TCE}}$  was estimated to be  $3.03 \times 10^{-2}$  cm<sup>2</sup>/h (20°C) [Hayduk and Laudie, 1974]. The dispersion coefficients for each interstitial velocity are evaluated from (2) and (3), respectively. Furthermore, the first-order decay constant is equal to zero ( $\lambda = 0$ ) because the presence of sodium azide in the influent clear well of the model aquifer prevented any possible biological degradation of TCE. The nonlinear least squares regression program PEST [Doherty et al., 1994] was employed for the estimation of the unknown overall mass transfer coefficient by fitting the analytical solution (19) to the observed aqueous phase TCE concentrations. For this study, only  $k^*$  was fitted because all of the other required model parameters were determined independently. The corresponding overall mass transfer coefficients for each sampling data set are listed in Table 1. The uncertainty of the fitted parameters was determined by estimating the corresponding 95% confidence intervals. It should be noted that for each interstitial velocity the estimated  $k^*$  values are practically identical, as expected at steady state conditions.

For the first experiment the observed concentrations at port 95 were consistently greater than expected for the medium interstitial velocity. For both the second and third experiments, port 95 yielded observed concentrations slightly less than those observed at port 63. This is reasonable because ports 63 and 95 are offset equal distances from the centerline and are at the same elevation, yet port 95 is 15 cm down gradient from port 63. Thus it appears that port 95 is not a flawed sampling

station. Instead, the elevated concentrations may have been caused by a temporary intrusion of nonaqueous phase TCE into the porous medium (in the vicinity of grid location 5, for example). However, the amount would have had to be minor because subsequent samples collected for the second and third experiments exhibit a return to more reasonable values.

The observed dissolved TCE concentrations at sampling locations 4, 34, and 144, along the centerline of the aquifer in the  $x$ - $z$  plane are compared to predictions based on the analytical solution (19)–(24) for  $U_x = 0.25, 0.75,$  and  $1.96$  cm/h (Figure 8). Model simulations are based on the average of the two fitted  $k^*$  values obtained for each interstitial velocity. The solid circles represent sampling locations, and the bold number next to each sampling location represents the corresponding average of the two observed TCE concentrations obtained for each interstitial velocity. Figure 8 clearly shows good agreement between the observed dissolved TCE concentrations and the analytical solution.

The experimentally determined overall mass transfer coefficients are compared to predictions obtained by a correlation for circular DNAPL pools developed by Kim and Chrysikopoulos [1999]. The correlation relates the overall Sherwood number  $Sh^*$  to the overall Peclet numbers of a circular pool in  $x$  and  $y$  directions  $Pe_x^*$  and  $Pe_y^*$ , respectively, as follows:

$$Sh^* = 1.74(Pe_x^*)^{0.33}(Pe_y^*)^{0.40}, \quad (25)$$

$$Sh^* = \frac{k_c^*(\pi^{1/2}r)}{\mathcal{D}_e}, \quad (26a)$$

$$Pe_x^* = \frac{U_x r}{D_x}, \quad (26b)$$

$$Pe_y^* = \frac{U_y r}{D_y}, \quad (26c)$$

where  $k_c^*$  is the correlation-determined time-invariant overall mass transfer coefficient. The preceding correlation is based on numerically determined overall mass transfer coefficients and is valid for  $U_x$  in the range from 0.42 to 4.2 cm/h. For the TCE dissolution experimental conditions of this study ( $\mathcal{D}_e^{\text{TCE}} = 0.0212$  cm<sup>2</sup>/h,  $\alpha_L = 0.259$  cm,  $\alpha_T = 0.019$  cm, and  $r = 3.8$  cm), correlation (25) predicts that  $k_c^* = 0.051, 0.074,$  and  $0.091$  cm/h for  $U_x = 0.25, 0.75,$  and  $1.96$  cm/h, respectively. Thus the experimentally evaluated and correlation-determined overall mass transfer coefficients agree to within a factor of 2. It should be noted that predictions based on correlation (25) are approximate because this relationship was developed by numerically generated data. The average of the two experimentally estimated  $k^*$  values obtained for each of the interstitial velocities examined in this work and those predicted by correlation (25),  $k_c^*$ , are presented in Figure 9.

## 6. Summary and Conclusions

A three-dimensional, bench-scale model aquifer was constructed to study the dissolution of a TCE pool. The aquifer consisted of medium-sized sand packing conveying steady, unidirectional flow. A key aspect of the experimental design was a mechanism by which a TCE pool of an ideal (circular) geometry was placed and maintained in direct contact with the bottom of the porous medium. The aqueous plume emanating from this pool was monitored at several downgradient sampling stations and analyzed using the analytical solution de-

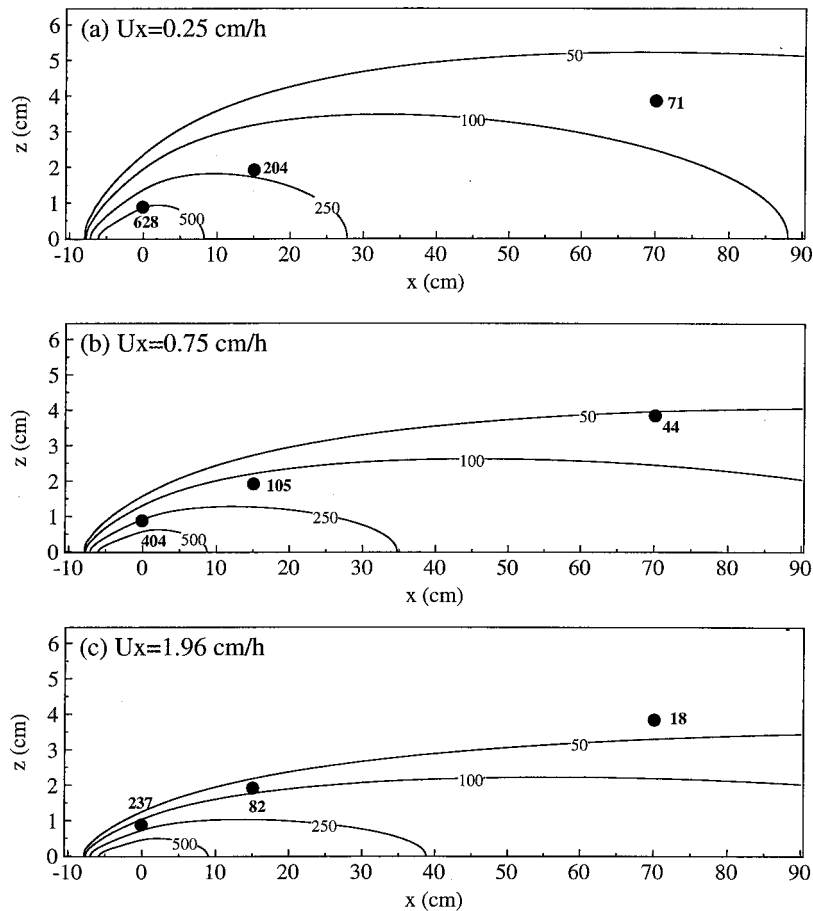


**Figure 8.** Steady state aqueous phase TCE concentration contour plots, along the centerline of the aquifer in the  $x$ - $z$  plane, generated for average  $k^*$  values by the analytical solution (19)–(24) and average observed concentrations at sampling locations indicated by the solid circles for (a)  $U_x = 0.25$  cm/h, (b)  $U_x = 0.75$  cm/h, and (c)  $U_x = 1.96$  cm/h. The center of the circular pool is at location  $x = -3.8$  and  $y = z = 0$  cm.

rived by *Chrysiopoulos* [1995]. All transport parameters required by this solution, with the exception of the average mass transfer coefficient ( $k^*$ ) for the pool, were estimated independently. Of special note are the dispersion parameters, which were estimated independently by fitting the results of a bromide tracer test with a newly derived analytical solution describing the transport of a conservative tracer in a homogeneous aquifer of finite thickness.

The analytical solution for pool dissolution was found to describe observed TCE plumes well. This result demonstrates that the model accurately describes the dynamics of the pool dissolution process. It confirms the hypothesis that the plumes generated from dissolving pools of infinite mass will achieve a steady state distribution. A constant mass flux develops at the pool-water interface and acts as the plume source. This flux is balanced by hydrodynamic conditions, which dilute the plume to below detection limits at the plume extremities. The experimental mass transfer coefficients obtained in this study can be used in field cases involving relatively homogeneous subsurface formations contaminated by TCE pools.

Observed aqueous TCE concentrations only 15–60 cm down gradient from the pool, and just a few cm above the pool elevation, were <4% of the aqueous solubility for TCE. This result provides strong evidence in support of the notion that the rate-limited dissolution of DNAPLs can be the cause of contaminant plumes that are dominated by concentrations sev-

eral orders of magnitude less than the aqueous solubility. The result also implies that observed concentrations exclusively at the parts per billion level do not preclude the existence of a DNAPL at a site.

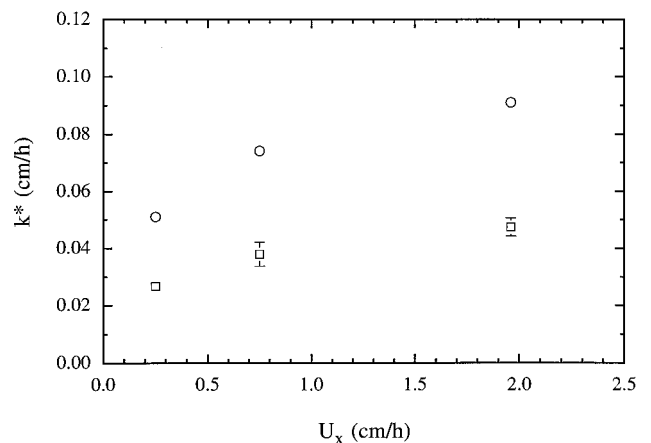


**Figure 9.** Comparison between experimentally determined overall mass transfer coefficients (squares) and those predicted by correlation (25) (circles). Error bars represent the 95% confidence intervals.

The testing procedure and results described in this work begin to validate an existing model describing dissolution from a DNAPL pool source in a more physically realistic manner. As an analytical solution, this model is easily implemented and may be useful for estimating pool size, location, and projected longevity under relatively homogeneous conditions. It must be emphasized that the experimental conditions for the pool placement in this work were tailored to the conditions imposed by the analytical solution. Real pools will shrink with time, and the interfacial area available to dissolution may change accordingly.

## Notation

$a$	major semi-axis of elliptic pool, $L$ .
$b$	minor semi-axis of elliptic pool, $L$ .
$C$	liquid phase solute concentration (solute mass/liquid volume), $M/L^3$ .
$C_s$	aqueous saturation concentration (solubility), $M/L^3$ .
$\mathcal{D}$	molecular diffusion coefficient, $L^2/T$ .
$\mathcal{D}_e$	effective molecular diffusion coefficient, equal to $\mathcal{D}/\tau^*$ , $L^2/T$ .
$D_x$	longitudinal hydrodynamic dispersion coefficients, $L^2/T$ .
$D_y$	lateral hydrodynamic dispersion coefficients, $L^2/T$ .
$D_z$	vertical hydrodynamic dispersion coefficient, $L^2/T$ .
$\text{erf}[\eta]$	error function, equal to $(2/\pi^{1/2}) \int_0^\eta e^{-\zeta^2} d\zeta$ .
$F$	general functional form of tracer source configuration, $M/L^3 T$ .
$G$	tracer release rate from a point source, $M/T$ .
$H$	finite water-saturated aquifer thickness, $L$ .
$k^*$	time-invariant overall mass transfer coefficient, $L/T$ .
$k_c^*$	correlation determined time-invariant overall mass transfer coefficient, $L/T$ .
$K_d$	distribution coefficient, $L^3/M$ .
$\ell_{x_0}, \ell_{y_0}$	$x$ and $y$ Cartesian coordinates, respectively, of the center of a circular pool, $L$ .
$m$	integer summation index.
$n_1, n_2$	defined in (22) and (23), respectively.
$Pe_x^*, Pe_y^*$	overall Peclet numbers of a circular pool in $x$ and $y$ directions, defined in (26b) and (26c), respectively.
$Q$	volumetric flow rate, $L^3/T$ .
$r$	radius of circular pool, $L$ .
$R$	dimensionless retardation factor.
$Sh^*$	time invariant overall Sherwood number, defined in (26a).
$t$	time, $T$ .
$U_x$	average groundwater velocity, $L/T$ .
$v$	defined in (24).
$w$	width of experimental aquifer, $L$ .
$x, y, z$	spatial coordinates, $L$ .
$x_0, y_0, z_0$	$x, y,$ and $z$ Cartesian coordinates, respectively, of a point source, $L$ .
$\alpha_L, \alpha_T$	longitudinal and transverse dispersivities, respectively, $L$ .
$\delta(\cdot)$	Dirac delta function.
$\zeta, \eta$	dummy variables.
$\theta$	porosity (liquid volume/aquifer volume), $L^3/L^3$ .
$\lambda$	decay coefficient, $T^{-1}$ .
$\mu$	dummy integration variable.

$\mu_1, \mu_2$	defined in (20) and (21), respectively.
$\rho_b$	sand bulk density, $M/L^3$ .
$\tau$	dummy integration variable.
$\tau^*$	tortuosity coefficient ( $\geq 1$ ).

**Acknowledgments.** This research was sponsored by the Environmental Protection Agency, under grant R-823579-01-0. However, the manuscript has not been subjected to the Agency's peer and administrative review and therefore does not necessarily reflect the views of the Agency, and no official endorsement should be inferred. Additional support from the University of California, Irvine, for the purchase and maintenance of the constant temperature chamber is gratefully acknowledged. The authors thank Mike Tatalovich for contributing to the tank construction.

## References

- Anderson, M. R., R. L. Johnson, and J. F. Pankow, Dissolution of dense chlorinated solvents into groundwater, 3, Modeling contaminant plumes from fingers and pools of solvent, *Environ. Sci. Tech.*, 26(5), 901–908, 1992.
- Bear, J., and A. Verruijt, *Modeling Groundwater Flow and Pollution*, D. Reidel, Norwell, Mass., 1987.
- Bennett, C. O., and J. E. Myers, *Momentum, Heat, and Mass Transfer*, 3rd ed., 832 pp., McGraw-Hill, New York, 1982.
- Chrysiopoulos, C. V., Artificial tracers for geothermal reservoir studies, *Environ. Geol.*, 22, 60–70, 1993.
- Chrysiopoulos, C. V., Three-dimensional analytical models of contaminant transport from nonaqueous phase liquid pool dissolution in saturated subsurface formations, *Water Resour. Res.*, 31(4), 1137–1145, 1995.
- Chrysiopoulos, C. V., and T.-J. Kim, Local mass transfer correlations for nonaqueous phase liquid pool dissolution in saturated porous media, *Transp. Porous Media*, 38(1/2), 167–187, 2000.
- Chrysiopoulos, C. V., and K. Y. Lee, Contaminant transport resulting from multi-component nonaqueous phase liquid pool dissolution in three-dimensional sub-surface formations, *J. Contam. Hydrol.*, 31, 1–21, 1998.
- Chrysiopoulos, C. V., E. A. Voudrias, and M. M. Fyrrillas, Modeling of contaminant transport resulting from dissolution of nonaqueous phase liquid pools in saturated porous media, *Transp. Porous Media*, 16(2), 125–145, 1994.
- de Marsily, G., *Quantitative Hydrogeology, Groundwater Hydrology for Engineers*, 440 pp., Academic, San Diego, Calif., 1986.
- Doherty, J., L. Brebber, and P. Whyte, PEST: Model-independent parameter estimation, Watermark Computing, Brisbane, Queensl., Australia, 1994.
- Domenico, P. A., and F. W. Schwartz, *Physical and Chemical Hydrogeology*, 824 pp., John Wiley, New York, 1990.
- Gelhar, L. W., Stochastic subsurface hydrology from theory to applications, *Water Resour. Res.*, 22(9), 135S–1145S, 1986.
- Geller, J. T., and J. R. Hunt, Mass transfer from nonaqueous phase organic liquids in water-saturated porous media, *Water Resour. Res.*, 29(4), 833–845, 1993.
- Gershon, N. D., and A. Nir, Effects of boundary conditions of models on tracer distribution in flow through porous mediums, *Water Resour. Res.*, 5(4), 830–839, 1969.
- Hayduk, W., and H. Laudie, Prediction of diffusion coefficients for nonelectrolytes in dilute aqueous solutions, *AIChE J.*, 20(3), 611–615, 1974.
- Holman, H.-Y. N., and I. Javandel, Evaluation of transient dissolution of slightly water-soluble compounds from a light nonaqueous phase liquid pool, *Water Resour. Res.*, 32(4), 915–923, 1996.
- Illangasekare, T. H., J. L. Ramsey Jr., K. H. Jensen, and M. B. Butts, Experimental study of movement and distribution of dense organic contaminants in heterogeneous aquifer, *J. Contam. Hydrol.*, 20, 1–25, 1995.
- Imhoff, P. T., P. R. Jaffé, and G. F. Pinder, An experimental study of complete dissolution of a nonaqueous phase liquid in saturated porous media, *Water Resour. Res.*, 30(2), 307–320, 1994.
- Jia, C., K. Shing, and Y. C. Yortsos, Advective mass transfer from stationary sources in porous media, *Water Resour. Res.*, 35(11), 3239–3251, 1999.
- Johnson, R. L., and J. F. Pankow, Dissolution of dense chlorinated

- solvents into groundwater, 2, Source functions for pools of solvent, *Environ. Sci. Technol.*, 26(5), 896–901, 1992.
- Khachikian, C., and T. C. Harmon, Nonaqueous phase liquid dissolution in porous media: Current state of knowledge and research needs, *Transp. Porous Media*, 38(1/2), 3–28, 2000.
- Kim, T.-J., and C. V. Chrysikopoulos, Mass transfer correlations for nonaqueous phase liquid pool dissolution in saturated porous media, *Water Resour. Res.*, 35(2), 449–459, 1999.
- Lee, K. Y., and C. V. Chrysikopoulos, Numerical modeling of three-dimensional contaminant migration from dissolution of multicomponent NAPL pools in saturated porous media, *Environ. Geol.*, 26, 157–165, 1995.
- Lee, K. Y., and C. V. Chrysikopoulos, NAPL pool dissolution in stratified and anisotropic porous formations, *J. Environ. Eng.*, 124, 851–862, 1998.
- Lindstrom, F. T., R. Haque, V. H. Freed, and L. Boersma, Theory on the movement of some herbicides in soils, linear diffusion and convection of chemicals in soils, *Environ. Sci. Technol.*, 1(7), 561–565, 1967.
- Mackay, D., W. Y. Shiu, and K. C. Ma, *Illustrated Handbook of Physical-Chemical Properties and Environmental Fate for Organic Chemicals, Volatile Organic Chemicals*, vol. 3, 916 pp., Lewis, Chelsea, Mich., 1992.
- Mason, A. R., and B. H. Kueper, Numerical simulation of surfactant-enhanced solubilization of pooled DNAPL, *Environ. Sci. Technol.*, 30, 3205–3215, 1996.
- Pearce, A. E., E. A. Voudrias, and M. P. Whelan, Dissolution of TCE and TCA pools in saturated subsurface systems, *J. Environ. Eng.*, 120, 1191–1206, 1994.
- Powers, S. E., L. M. Abriola, and W. J. Weber Jr., An experimental investigation of nonaqueous phase liquid dissolution in saturated subsurface systems: Steady state mass transfer rates, *Water Resour. Res.*, 28(10), 2691–2705, 1992.
- Seagren, E. A., B. E. Rittman, and A. J. Valocchi, An experimental investigation of NAPL-pool dissolution enhancement by flushing, *J. Contam. Hydrol.*, 37, 111–137, 1999a.
- Seagren, E. A., B. E. Rittman, and A. J. Valocchi, A critical evaluation of the local-equilibrium assumption in modeling NAPL-pool dissolution, *J. Contam. Hydrol.*, 39, 109–135, 1999b.
- Sim, Y., and C. V. Chrysikopoulos, Analytical solutions for solute transport in saturated porous media with semi-infinite or finite thickness, *Adv. Water Resour.*, 22(5), 507–519, 1999.
- Voudrias, E. A., and M. F. Yeh, Dissolution of a toluene pool under constant and variable hydraulic gradients with implications for aquifer remediation, *Groundwater*, 32(2), 305–311, 1994.
- Whelan, M. P., E. A. Voudrias, and A. Pearce, DNAPL pool dissolution in saturated porous media: Procedure development and preliminary results, *J. Contam. Hydrol.*, 15(3), 223–237, 1994.
- 
- C. V. Chrysikopoulos, Department of Civil and Environmental Engineering, University of California, Irvine, Irvine, CA 92697-2175. (costas@eng.uci.edu)
- T. C. Harmon, Department of Civil and Environmental Engineering, University of California, Los Angeles, Los Angeles, CA 90095-1593.
- K. Y. Lee, Department of Civil and Environmental Engineering, Rutgers, The State University of New Jersey, Piscataway, NJ 08854. (kenlee@rci.rutgers.edu)

(Received November 8, 1999; revised March 13, 2000; accepted March 23, 2000.)